Limitations of the distorted-wave impulse approximation in describing the energy dependence of the ^{10}B$(n, p)^{10}$Be (g.s.) reaction

D. S. Sorenson, J. L. Ullmann, A. Ling, B. K. Park, R. C. Haight, and N. S. P. King
Los Alamos National Laboratory, Los Alamos, New Mexico 87544, USA

R. A. Lindgren and H. Baghaei
University of Virginia, Charlottesville, Virginia 22901, USA

E. J. Stephenson
Indiana University Cyclotron Facility, Bloomington, Indiana 47408, USA

F. P. Brady and J. L. Romero
University of California, Davis, California 95616, USA

J. Rapaport
Ohio University, Athens, Ohio 45701, USA

B. L. Clausen
Geoscience Research Institute, Loma Linda University, Loma Linda, California 92350, USA

C. Wuest
Lawrence Livermore National Laboratory, Livermore, California 94550, USA

F. Sammarruca
University of Idaho, Moscow, Idaho 83844, USA
(Received 14 November 2006; published 21 March 2007)

We report differential cross section measurements for the stretched transition from the ^{10}B ground state ($J^\pi = 3^+$) to the ^{10}Be ground state ($J^\pi = 0^+$) in the ^{10}B$(n, p)^{10}$Be (g.s.) reaction. These data were obtained over the energy range from 70 to 240 MeV, covering momentum transfer values from 0.6 to 2.5 fm^{-1}. In this momentum transfer range, the isovector tensor effective interaction dominates the transition. Cross sections are compared to zero- and finite-range distorted wave impulse approximation calculations using modern free and density-dependent effective interactions and a transition density consistent with (e, e') data. Good agreement is observed at energies above 120 MeV, but below this energy the cross sections are larger than the calculated values by more than 40%. The implications for DWIA calculations are discussed.

DOI: 10.1103/PhysRevC.75.034611 PACS number(s): 25.40.Kv, 24.10.Eq, 27.20.+n

I. INTRODUCTION

The major tool for describing the reaction mechanism of nucleon-induced inelastic scattering and charge exchange at intermediate energies (above 50 MeV) is the distorted wave impulse approximation (DWIA). The DWIA is a single-step calculation where the transition potential is replaced by an effective interaction fitted to the nucleon-nucleon (NN) scattering amplitudes. This is well known to reduce the size of the perturbation and improve the accuracy in the single-step calculation [1]. In addition, there are many cases where the nuclear structure of the transition is also well known, often from a combination of shell model considerations and inelastic electron scattering data. This makes possible tests that explore the limits of the DWIA and point toward ways that it can be improved. Here we will present measurements of the energy dependence of the ^{10}B$(n, p)^{10}$Be(g.s.) differential cross section between 70 and 240 MeV and show how this allows us to explore the transition from a regime of good agreement at the higher energies to much poorer agreement at the lower energies.

It is crucial to such an endeavor that the underlying NN interaction reproduces NN data to high precision [2–5], especially in recent experiments in this energy range ([6–8], which supersede [9]). An effective NN interaction for DWIA calculations can now be constructed that includes the medium effects of Pauli blocking, nuclear binding, and relativity [10–12]. (The addition of meson spectral properties [13] or Δ-isobars [14] would also seem to be well motivated, but is not needed to match nuclear matter properties [15].)

At the same time, there are many nuclear transitions whose structure is particularly simple and well understood. This structure is often described within DWIA as a summation over the contributing particle-hole pairs that represent the transition to the excited state of the target nucleus. In the case described in this paper, we will be considering a "stretched" transition in which the particle and hole spins are maximally aligned

($J_{\rm tr} = j_p + j_h = \ell_p + \ell_h + 1$). If the hole state comes from a valence orbital that is also the highest angular momentum orbital in the nucleus, and if the transition goes to another orbital of that angular momentum or higher, then there is essentially only one particle-hole configuration that can contribute. This eliminates the difficulty of obtaining the relative strengths of different particle-hole terms, and it allows the amplitude and shape of the wave functions that make up the transition density to be determined from electron scattering measurements.

In the case of the ^{10}B$(n, p)^{10}$Be(g.s.) transition there are additional restrictions on the parts of the effective NN interaction that are allowed to participate. The charge-exchange nature of the reaction plus the isospin of the target ($T = 0$) requires that only isovector amplitudes appear in the effective NN interaction. The unnatural parity ($J^\pi = 3^+$) of the transition also eliminates any participation by spin-independent amplitudes. What is left comes mainly from the tensor force, mediated mostly by the pion and reduced at short range by the ρ-meson. Spin-spin contributions, which appear at lower energies and lower momentum transfers, are relatively minor, and spin-orbit contributions are almost inconsequential. The resulting tensor effective NN interaction is well constrained, particularly by polarization observables in the NN system, and roughly independent of energy [16]. This part of the effective NN interaction is also relatively unaffected (compared to isoscalar central and spin-orbit terms) by modifications arising from the nuclear medium [17]. This provides an interaction that is very well known. Because the spin operators for the direct and exchange parts of the tensor interaction are different, finite-range DWIA calculations are usually necessary for a faithful reproduction of the effects of the exchange amplitude. However, the zero-range approximation becomes better as the angular momentum transfer increases and gives a quantitatively useful prediction even at $J_{\rm tr} = 3$. In Sec. III we will compare zero- and finite-range DWIA calculations.

The analog ^{10}B$(e, e')^{10}$B (1.74 MeV) transition has been measured to particularly high momentum transfers in transverse electron scattering [18]. The momentum transfer dependence constrains the radius and diffuseness of a Woods-Saxon potential used to provide the nuclear $p_{3/2}$ wave functions for the particle and hole involved in this 3^+ transfer. The size of the (e, e') cross section also gives the normalization of the transition density. Assuming isospin is a good quantum number, we can take the shape and magnitude of the transition density from the (e, e') measurements and use them to set the scale of the (n, p) cross section that is the crucial focus of this paper. Once this scale has been established, we will find good agreement with the measurements at the upper end of the energy scale and progressive divergence as the energy goes down.

The experiment that we describe in the next section utilized the white neutron source at the Los Alamos National Laboratory. Unique to this facility is the ability to make cross section measurements simultaneously over a broad energy span, thus eliminating relative normalization issues when looking at the energy dependence of the tensor force. The fact that the stretched transition in the ^{10}B$(n, p)^{10}$Be reaction goes to the ground state of ^{10}Be and our energy resolution is sufficient to separate the ground state transition from other nuclear states means that the background in the detection of the outgoing protons is small. Angular distributions were separated into six energy bins with centers between 70 and 240 MeV. These data covered the momentum transfer range from 0.6 to 2.5 fm^{-1}.

Originally, the measurements of the (n, p) cross section were compared to zero-range DWIA calculations based on the Franey-Love interaction [19]. This showed that between 70 and 240 MeV the ratio of the measured cross section to the calculation fell by over 40% when it was expected to remain unchanged. The Franey-Love interaction was based on an earlier energy-dependent phase shift analysis by Arndt [20] that resulted in a particularly low value of the $J = 1$ mixing parameter, ε_1 (see Table IV of Ref. [20]), at the lower energies. This raised the question of whether the disagreement was a result of this feature of the description of the tensor interaction. So the analysis was repeated with a more modern interaction [11] that is an improved version of the Bonn-B potential [15] with excellent reproduction of the NN observables below the pion production threshold. In addition, the zero-range calculations made earlier were repeated with full finite range in order to properly include the effects of particle exchange, an important feature in the description of the tensor force. Lastly, Pauli blocking and dispersion effects were added. The last change made some improvement in the description of the energy dependence compared to the use of a modern free interaction. But inconsistencies in the normalization as large as 45% still remain across the low energy range.

The implications of the above result are considered by making consistency checks with the constraints on the tensor interaction provided by the NN data. It is shown that leeway to accommodate a 45% effect does not exist. Thus the problem must represent a limit on the applicability of the DWIA to handle nucleon-induced reactions at the lower energies studied here. To further explore this limit, we compare the energy dependence of the ^{10}B$(n, p)^{10}$Be reaction with the results for unnatural-parity isovector transitions measured with (p, p') and (p, n) reactions on neighboring nuclei. We find a range above mass 20 where good agreement with the DWIA energy dependence is obtained. This allows us to set bounds in energy and mass on the validity of DWIA calculations of isovector tensor transition strength and leads us to suggest possible improvements of DWIA reaction models. The paper is organized as follows: The details of the experiment and cross section measurements for the ^{10}B$(n, p)^{10}$Be(g.s.) reaction are given in Sec. II. Comparisons of the DWIA calculations using various model parameters are compared to the data in Sec. III. The conclusions of the paper are given in Sec. IV.

II. EXPERIMENTAL RESULTS

The experiment was conducted at the Weapons Neutron Research Facility [21] located at Los Alamos National Laboratory. This facility makes use of the Clinton P. Anderson Accelerator Facility 800-MeV proton beam. The pulsed and bunched proton beam was focused onto a 7.5-cm thick tungsten

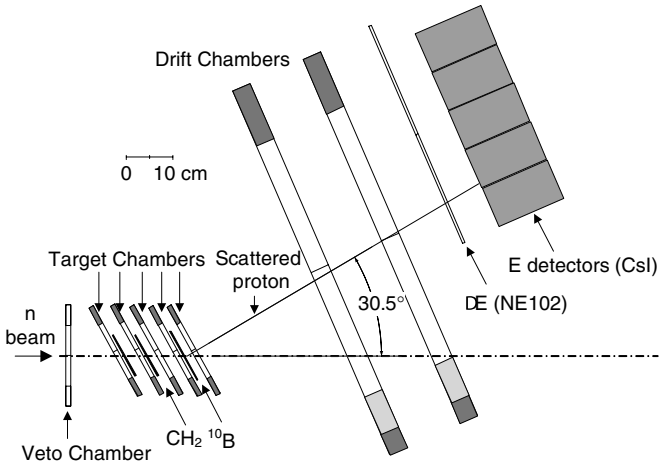

FIG. 1. Top view of experimental geometry. See text for a detailed description.

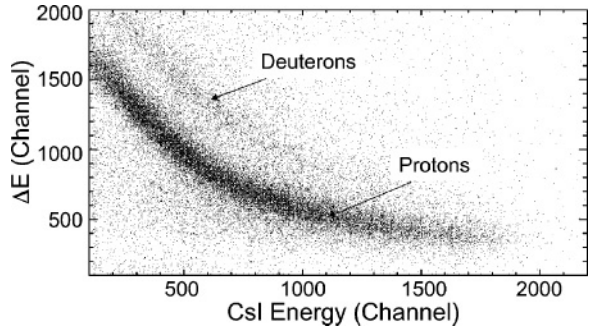

FIG. 2. Scatter plot of Delta E from the NE102 scintillator versus energy from the CsI detector. Loci for deuterons and protons are shown.

target producing a pulsed white neutron flux with energies up to 800 MeV. The experiment was located 90 m from the production target where time-of-flight techniques could be used to determine the neutron energy.

The detection system used to obtain the data has been used for other experiments [22,23] but was modified in this case as described below. Figure 1 shows the view looking down on the experimental arrangement. The solid angle varies depending on the target being analyzed. In the figure a trajectory is shown from the ^{10}B target (fourth target position) with a horizontal scattering angle of 30°. The total solid angle given by the CsI detector array and the ^{10}B target position is approximately 240 msr (vertical angle acceptance ranges from $-12°$ to $+12°$ and the horizontal angle acceptance ranges from 15° to 50°). The neutron beam is shown going from left to right and has been collimated to a square beam with an area of 10×10 cm^2. For this setup, up to four targets can be studied simultaneously using the neutron beam. Each target has an associated wire chamber (15×15 cm^2) located directly downstream which was used to identify the target in which any charged particle producing reaction occurred. An additional wire chamber (veto chamber) was used upstream to tag any charged particles that remained in the neutron beam. In addition to the veto chamber, permanent magnets located along the flight path were used to sweep charged particles out the beam as well. The 180 mg/cm^2 ^{10}B enriched target was 91.5% ^{10}B by weight and was located in the fourth target position as shown in the figure. Charged particles originating from the target pass through two large area drift chambers (58×32 cm^2), a thin (0.50 cm) NE102 scintillator and finally deposit energy in one of the 15 CsI(Tl) ($8.9 \times 8.9 \times 15.2$ cm^3) detectors. The CsI detectors are stacked into an array of three tall by five wide as shown in Fig. 1. The thickness of the CsI can stop a proton with a maximum energy of 260 MeV. The higher energy protons pass through the CsI depositing less energy. The drift chambers shown allow the two dimensional position of the charged particle to be determined to a precision of 125 micron (FWHM) in the plane of the drift chambers. From the two positions given by the drift chambers, the angle can be determined by extending a line through the two points and calculating the angle between the beam axis and the charged particle trajectory.

Particle identification is determined by measuring the energy deposited in the thin NE102 scintillator and the total energy deposited in the CsI detector. By plotting these two variables the proton and deuteron particles can be easily discriminated as shown in Fig. 2. Protons with energies larger than 260 MeV are not observed in this plot because a neutron energy cut has been placed on the incoming neutron energy, which is independently measured through time of flight techniques. The intrinsic resolution of the CsI crystal, the neutron time of flight, target thickness and straggling all contribute to the proton energy resolution. The neutron beam energy resolution (FWHM) varies from 0.2 MeV for 40 MeV neutrons to 1.8 MeV for 260 MeV neutrons.

Typical proton energy spectra near the peak of the (n,p) cross section (laboratory angle of 24°) are shown in Fig. 3 for the six neutron energy bins used in this experiment. The data show peaks corresponding to transitions to the ^{10}Be ground state and to the first excited 2^+ state at 3.4 MeV. The curves for the peak shapes are guides to the eye, not fits for peak sums. Cross sections were based on sums of the spectra over the region representing the ground state peak. The incident neutron energies were binned in intervals of 20 MeV from 60 to 100 MeV and in intervals of 40 MeV from 100 to 260 MeV. Proton emission angles were binned in 4° intervals. The energy binning is acceptable for this particular reaction because the differential cross section varies slowly over this energy range.

The ^{10}B target has a few contaminants. The first is ^{11}B which contributes 8.5% by weight to the target. The protons from the ^{11}B$(n, p)^{11}$Be(g.s.) reaction (Q-value of -10.727 MeV) are well separated in energy from the protons that result from the ^{10}B$(n, p)^{10}$Be(g.s.) reaction (Q-value $= 0.226$ MeV) and therefore do not fall into the peak of interest. In addition, there is a small percentage ($\approx$5%) of H and C due to the binder. For these contaminants, the kinematics are such that the protons from C(n, p) and H(n, p) reactions do not interfere with the energy peak of interest for most of the energies and angles in this analysis. Corrections were required for the averages energies of 70, 90, and 120 MeV and average laboratory angles of 20.4, 24.1, and 27.9 degrees. These corrections were typically around 5% except for the cases at 70 and 90 MeV at

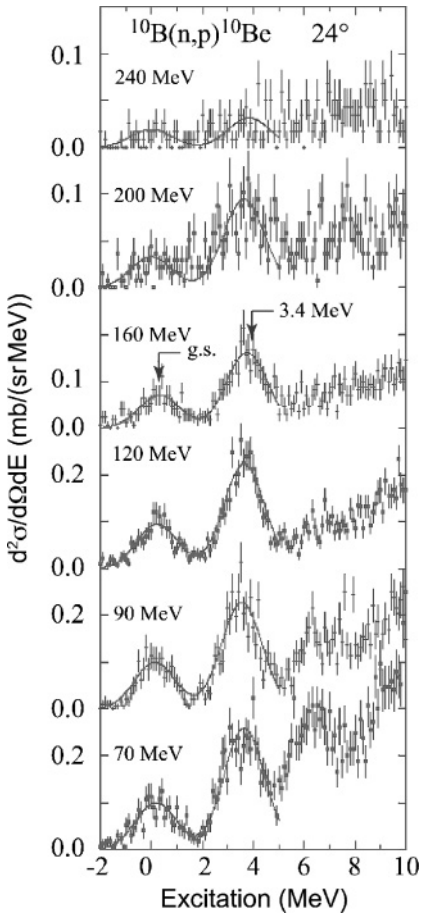

FIG. 3. The ^{10}B$(n, p)^{10}$B excitation energy spectra at a laboratory angle of 24° and at average neutron energies from 70 to 240 MeV. The ground state and 3.4 MeV transitions are easily resolved. The scales have been increased for the two largest energies.

20.4° in which a 20% and 10% correction respectively were determined.

Since the incident neutron flux is not measured in the experiment, the ^{10}B$(n, p)^{10}$Be(g.s.) cross sections are determined by normalizing to the H$(n, p)n$ cross sections. For the data presented here, the $n + p$ cross sections given by the SM99 phase shift solution of Arndt and Roper [24] were used for normalization. The (n, p) differential cross sections were calculated using

$$\frac{d\sigma}{d\Omega}(E_n, E_p, \theta,) = \frac{N(^{10}\mathrm{B})}{N(H)} \cdot \sigma_{n-p}(E_n, \theta) \frac{\left(\frac{\rho t}{A}\right)_{\mathrm{CH_2}}}{\left(\frac{\rho t}{A}\right)_{^{10}\mathrm{B}}} \cdot \frac{d\Omega^{T2}_{n-p}(\theta)}{d\Omega^{T4}_{^{10}\mathrm{B}}(\theta)} \cdot \frac{NI_{n-p}(E_{p'})}{NI_{^{10}\mathrm{B}}(E_p)}, \quad (1)$$

where the $N(A)$ are the number of events in the ^{10}B$(n, p)^{10}$Be(g.s.) and the H$(n, p)n$ peaks, ρt is the areal density of the target, $d\Omega$ is the solid angle, and NI is the nuclear interaction correction for CsI [25–27]. E_n and E_p are the neutron and proton energies in the (n, p) reaction while $E_{p'}$ is the energy of the proton from H$(n, p)n$ scattering. The ratio of the solid angles in Eq. (1) is typically close to one and accounts for the fact that the ^{10}B and CH_2 targets are in different positions along the neutron beam line. The ratio of the nuclear interaction corrections were within 10% of one for most of the angle and energy bins. The final data will be shown in the next section.

III. DWIA CALCULATIONS

In this section we will present a variety of DWIA calculations as they were developed historically. We start with a detailed discussion of the original zero-range calculations that incorporated the Franey-Love effective NN interaction [19]. These made use of the programs ALLWRLD [28] and TAMURA [29]. These calculations failed to reproduce the energy dependence of the ^{10}B$(n, p)^{10}$Be(g.s.) cross section. Subsequently, the question was raised whether this failure arose because of some inadequacy in either the reaction model or the isovector tensor part of the interaction. In order to address the importance of finite-range calculations for an adequate description of the exchange part of the tensor interaction, we switched to the program DWBA86 [30]. The older Franey-Love effective NN interaction was replaced with a more modern one, a variation on the Bonn-B potential that reproduced the modern NN database [11]. Lastly, medium modifications were included. We will review all of these efforts in this section and end with a summary of the DWIA situation in calculating the cross section for this transition.

A. Zero-range DWIA calculations

The zero-range calculations are similar to those presented by Baghaei [31] where the analog ^{10}B$(p, p')^{10}$B reaction to the 0^+ state at 1.74 MeV was studied with 200 MeV polarized protons. Up to effects caused by differences in the particle and hole binding energies, the nuclear transition densities are the same. The calculation follows the approach of Carpenter and collaborators [31–35]. The program ALLWRLD was used to calculate the optical potentials for the incoming neutron and outgoing proton channels by folding the transition densities with the NN effective interaction. Finally, these results were used as input into the DWIA program TAMURA where the differential cross sections were calculated.

The optical potentials were constructed by folding the Hamburg G-matrix [36,37] with Cohen and Kurath [38] shell model densities adjusted to reproduce the available weak and electromagnetic data and employing an approximate treatment of exchange. Baghaei [31] used these potentials to calculate proton elastic scattering from ^{10}B at 200 MeV and found reasonable agreement with the elastic scattering cross section data. A significant $J = 2$ multipole contribution was needed at angles past 30°. This $J = 2$ piece was not included in the calculation of the optical model wave functions as the critical parts for a DWIA calculation lie at smaller angles where the usual $J = 0$ piece dominates. The central real and imaginary optical potentials for the energies between 70 and

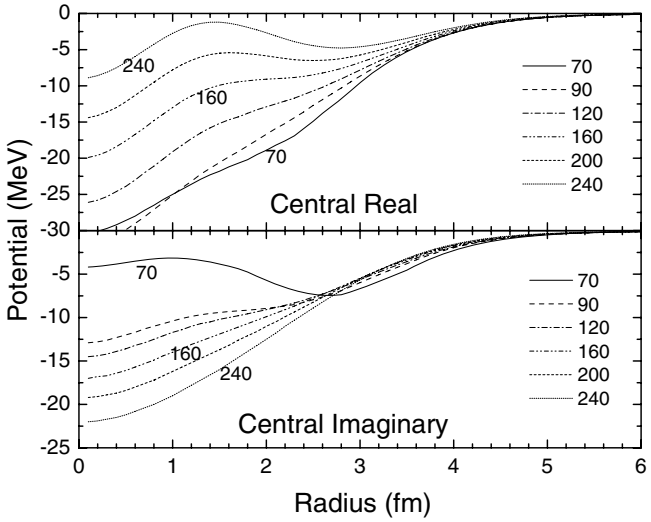

FIG. 4. Central real and imaginary optical potentials for the $n+^{10}$B channel folded from the Hamburg G-matrix.

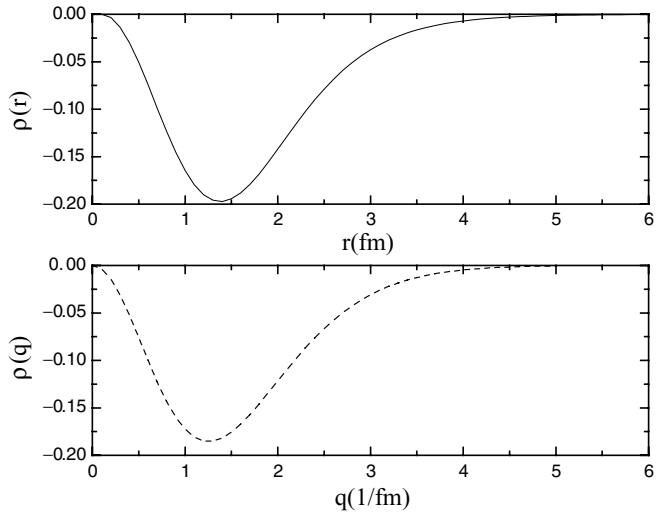

FIG. 6. Transition densities for $p(3/2) \rightarrow p(3/2)$ in coordinate and momentum spaces based on wavefunctions calculated for a Woods-Saxon potential.

240 MeV are shown in Fig. 4; the spin-orbit real and imaginary potentials are shown in Fig. 5. The real central potential curves show the progression from an attractive well at 70 MeV to a double peaked and small potential at 240 MeV as the $^1S_0$ NN phase shift moves toward its zero crossing near 250 MeV [2].

For the second part of the zero-range calculation, ALLWRLD was used to construct a scattering potential by folding the Franey-Love effective interaction [39] with the transition density. This density was described by a Woods-Saxon radial wave function [40,41] and Cohen and Kurath $(p_{3/2})^2$ shell model amplitudes [38]. The radius ($r_0 = 0.875$ fm) and diffuseness ($a_0 = 0.707$ fm) of the Woods-Saxon potential well were adjusted to reproduce the transverse electron scattering for the analog (e, e') transition in ^{10}B measured by Hicks [18]. For stretched transitions, the transition density $\rho^{s\perp}$ is related to the transverse electron form factor F_T through [42–46]:

$$|F_T|^2 = \frac{4\pi}{Z^2}\left(\frac{2J_f+1}{2J_i+1}\right)\left(\frac{q\hbar}{2Mc}\right)^2\left(\frac{g_\alpha^s}{2}\right)^2 |f_s\rho^{s\perp}|^2, \quad (2)$$

where g_α^s is the spin g factor and f_s is the proton charge form factor given by

$$f_s = \left(\frac{1}{1+\frac{0.76\cdot q^2}{12}}\right)^2. \quad (3)$$

The transition density is shown in Fig. 6 in both Cartesian and momentum spaces. Figure 7 shows the high quality of the agreement between the transverse form factor calculated using Eq. (2) and the data from the ^{10}B$(e, e')^{10}$B reaction to the state at 1.74 MeV, the analog to the state being considered here [18]. The normalization (spectroscopic amplitude of 0.257) of the calculated transverse form factor set the spectroscopic factor for the DWIA calculation. Small MEC corrections were not included in this fit to the data nor made to the data as they were in the previous work [2].

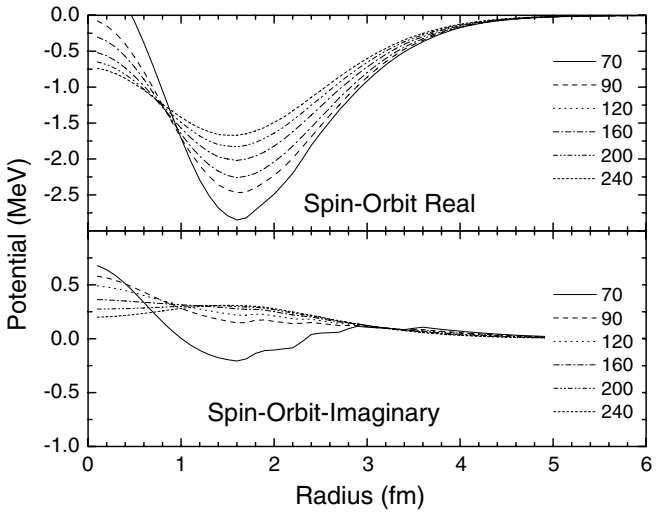

FIG. 5. Spin-orbit real and imaginary optical potentials for the $n+^{10}$B channel folded from the Hamburg G-matrix.

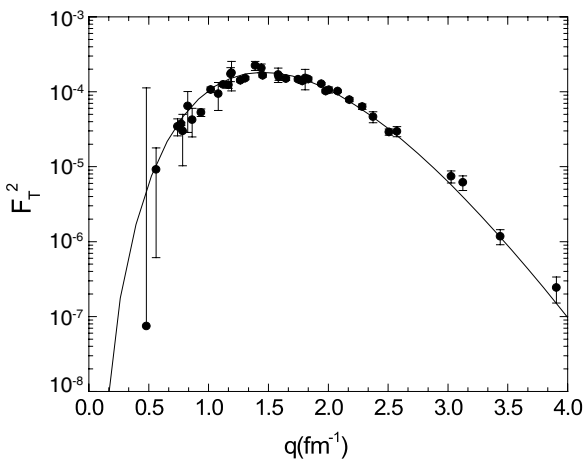

FIG. 7. Data for $|F_T|^2$ from the ^{10}B$(e, e')^{10}$B and a fit using Eq. (2).

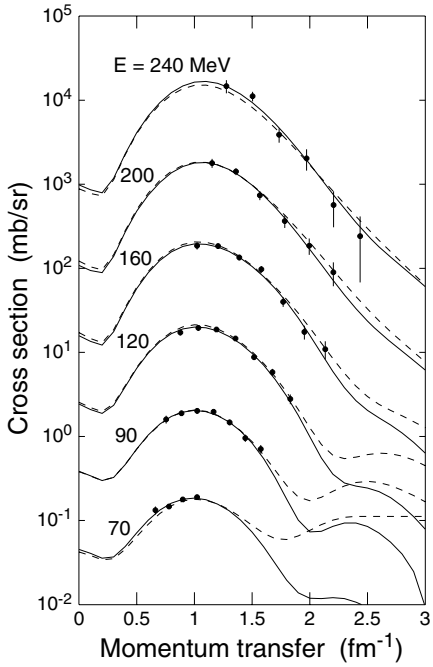

FIG. 8. Angular distributions of the ^{10}B(n, p)^{10}Be (g.s.) reaction. The cross sections have been binned into six energy bins ranging from 70 to 240 MeV. The zero-range DWIA calculations using the Franey-Love interaction (solid curve) and a modern free interaction (dashed curve) are shown with the data. Each successive energy is scaled up by a factor of 10.

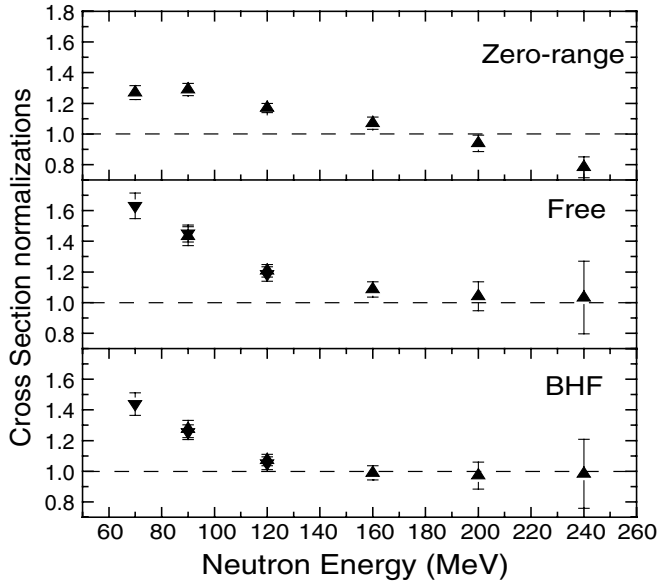

FIG. 9. Normalization factors used to scale the calculated cross section to the ^{10}B(n, p)^{10}Be reaction data. The calculations reflect the Franey-Love interaction and zero-range DWIA (top), a modern free interaction and finite-range DWIA (middle) and a BHF density-dependent interaction and finite-range DWIA (bottom).

Using the input provided by ALLWRLD, the program TAMVAX (a revised version of TAMURA) calculated the reaction cross sections in a zero-range approximation. The results for the isovector ^{10}B(n, p)^{10}Be reaction to the 0^+ final state are shown by the solid curves in Fig. 8. The interaction was taken from the closest of the preset energies of 100, 140, 175, and 210 MeV at which the published Franey-Love interaction is tabulated [19]. The quality of agreement shown in Fig. 8 required that the cross sections be renormalized by the factors plotted in the top panel of Fig. 9. The errors in these normalizations were estimated from a propagation of the errors in the cross sections themselves as they influence the choice of the normalization factor.

The shape of each cross section angular distribution is well reproduced. The changes to the normalization vary smoothly from a 30% increase at the lowest energies to a 20% decrease at the highest. If all other aspects of the DWIA calculations are correct, then one interpretation is that the strength of the NN tensor interaction should be renormalized as a function of energy to accommodate the differences shown in Fig. 9. Before we conclude that this is the only interpretation, we will investigate in the next subsection the quality of some of the approximations that go into the zero-range DWIA, and then consider the consistency of this result with what we know from analyses of NN data.

B. Improved DWIA calculations

The first question that we wish to address is whether the failure to obtain a uniform normalization as a function of energy is the fault of the Franey-Love interaction. For comparison, we switched to a more modern interaction [11] that reproduced the phase shift solution adopted by the Nijmegen group for NN energies below 325 MeV [47]. This interaction, an improvement of the Bonn-B potential [15], provided a reproduction of NN data that is comparable to CD-Bonn [4] or AV-18 [2]. The results, calculated with zero range, are shown as the dashed curves in Fig. 8. These curves have the same normalization as the zero-range Franey-Love calculations (solid curves). There is no significant difference between the quality of fit for the two sets of angular distributions that would allow us to choose one or the other on the basis of shape alone. Large differences between them are seen for the largest momentum transfers and the lowest energies, but there is no data with which to check these predictions. The general increase in the cross sections at higher momentum transfer may reflect the larger short-range tensor strength in the more modern interaction.

Next we checked the zero-range approximation by replacing it with a finite range treatment of the exchange parts of the DWIA integral. For this, we used a different program, DWBA86 [30]. As in the case with the zero-range calculation, the optical potential was generated by folding the effective interaction over the ground state density of ^{10}B. Because we finally wished to use density-dependent effective interactions, this folding was made with the zero-range program LEA [48]. The point nuclear density for ^{10}B was obtained from the charge density [49] by unfolding the contribution from the proton charge form factor [see Eq. (3)]. Both zero- and finite-range DWIA calculations (TAMURA and DWBA86) employed the same transition density adjusted in strength to match the transverse (e, e') data.

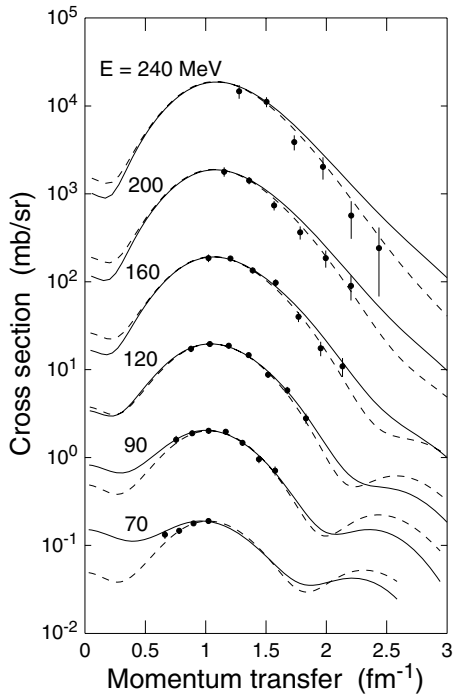

FIG. 10. Angular distributions displayed as in Fig. 8, but in comparison to finite-range DWIA calculations. The solid (dashed) lines make use of density-dependent (free) modern interactions.

Figure 10 shows the same data as Fig. 8, this time with calculations made using full finite range DWIA. The dashed curves make use of the same modern free interaction [11] that we just tested in zero range. Using finite range procedures reduced the large momentum transfer cross section, causing it to fall below even the zero-range Franey-Love treatment beyond the range of the data. The normalizations as a function of energy are shown in the middle panel of Fig. 9. For the finite range cases, the angular distribution shapes did not produce as small a value of chi square as we found for the zero-range case. So instead the curves were matched at a particular value of the momentum transfer. This was 1.0 fm^{-1} for 70, 90, and 120 MeV (down-pointing triangles in Fig. 9) and 1.2 fm^{-1} for 90 through 240 MeV (up-pointing triangles). The cross section for matching was obtained by extrapolating a Gaussian best-fit function that reproduced the angular distribution at each energy to the chosen momentum transfer. The overlaps between matching at the two values of momentum transfers at 90 and 120 MeV agree within errors. This procedure results in considerably larger errors for the normalization at the highest energies because the matching point is near the edge of the measured angular distribution. In spite of these larger errors, it is clear that the normalization no longer varies linearly with energy but now appears to approach a value of one as the energy rises (see Fig. 9 middle panel). Excellent agreement would be a value of one at all energies. The difference between the normalizations for 70 and 240 MeV remained the same. This shifts the concern to the lowest energies as the main source of the discrepancies with the tensor force that is provided by the effective NN interaction. So far, neither finite-range calculations nor a modern interaction have made any change in the size of the normalization problem across energy.

The solid curves in Fig. 10 include density dependence in the form of Pauli blocking and nuclear binding corrections (Brueckner-Hartree-Fock, or BHF) to the effective interaction [50]. Now the high-momentum parts of the angular distributions are noticeably larger than the measurements. Again because of the lack of a match to the angular distribution shape, the curves were normalized using the point matching scheme just described. These normalizations are shown in the bottom panel of Fig. 9. The curved shape of the normalizations noted before for the free interaction also is present here, but the factors at the lower energies are now somewhat smaller. While this improves the situation marginally, it does not represent an explanation of the change in normalization with neutron bombarding energy.

One curious feature of the density-dependent calculations is the flatter angular distribution at lower energies and momentum transfers. In order to learn the source of this at an incident energy of 70 MeV we separated in Fig. 11 the partial cross sections from each of the major components of the calculation alone: tensor (long dash), spin-orbit (dot-dash), and central (short dash). The original full calculation is shown again with a solid line. The top panel shows the free interaction while the lower panel the density-dependent one. First, the top calculation in particular confirms the original contention that this transition is dominated by the tensor part of the effective NN interaction. The next largest component, the central, is important only for the most forward angles. This component enters an unnatural parity transition only through the spin-spin operator. When density dependence is included, this central part increases in size, raising the forward angle cross section and tending to fill the valley in the forward angular distribution left by the tensor. It is this effect that causes the major change in the shape of the 70 MeV calculation. In neither case does the spin-orbit contribution become large enough to matter.

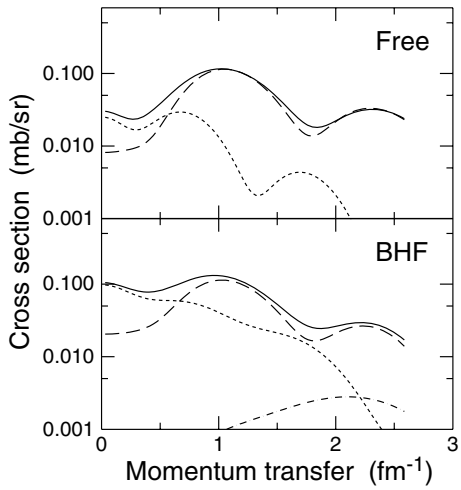

FIG. 11. Decomposition of the calculated 70-MeV free and BHF cross sections showing the total calculation (solid) and a cross section calculated from the amplitudes for just the tensor (long dash), central (short dash), and spin-orbit (dot-dash).

C. Further interpretations

The question raised by these apparently robust changes with bombarding energy in the renormalizations of the effective tensor interaction is whether they are compatible with the constraints from the NN scattering database. If so, it should be possible to reliably infer the size of the isovector NN tensor interaction strength from the charge exchange measurements. The effective interaction used in DWIA programs is usually expressed in either coordinate or momentum space as an expansion in Yukawa functions with different ranges [51]. The strength of each spin operator [$1, \sigma_1 \cdot \sigma_2, \sigma_1 + \sigma_2, S_{12}$ and S_{12}(Q)] is described with a separate expansion. In the case of the free interaction, these functions describe NN scattering and can be used to calculate NN observables or phase shifts. In the Yukawa form, it would be simple enough to increase the size of the tensor interaction alone to account for the rise in the normalization as the energy goes down. (Increasing the whole interaction would raise the NN cross section, creating a clear variance with NN data.) Unfortunately, the Yukawa expansion does not necessarily obey the constraints inherent in NN scattering (except insofar as its coefficients are adjusted to reproduce NN scattering amplitudes). For example, after such an increase, the phase shifts affected by the tensor force will no longer remain unitary (have an inelasticity parameter $\eta = 1$) and observables in the proton-proton channel will no longer be completely symmetric or anti-symmetric about $\theta_{\text{c.m.}} = 90^\circ$. This means that other changes to central and spin-orbit terms in the effective interaction would be required in order to maintain these basic properties. Such an investigation, perhaps through the use of a one-boson exchange model, is beyond the scope of this paper.

Nevertheless, we note that the NN mixing parameters vary almost linearly with the strength of the tensor force. So, despite the concerns already discussed, a simpler way to make a test for consistency is to ask whether the required changes are within the bounds that would be considered reasonable for the mixing parameters as determined from the fit to NN data. Whatever set of Yukawa functions is used to describe the effective NN interaction can be reexpressed as (complex) phase shifts by using the transformation in Appendix A of Ref. [11]. (When this is applied to a free interaction, one gets back the NN phase shifts on which the Yukawa expansion was based.) So the test would consist of changing the tensor Yukawa coefficients to produce agreement with the (n, p) cross section data and calculating the revised phase shifts from the altered effective interaction.

We chose the 70 MeV data and the modern free interaction for the test case, as the agreement here was the worst. Since a larger uncertainty is associated with the ε_1 parameter (which reflects the strength of the short-range tensor force) in the phase shift analysis, we increased the contribution from the shortest range Yukawa ($r = 0.15$ fm) term first. Then all tensor Yukawa coefficients were increased until the calculation matched the 70 MeV cross section data. The initial and final values of the first four mixing parameters are given in Table I along with the percentage increase. The initial increase in the shortest-range Yukawa contribution has clearly moved much of the load for reproducing the stronger tensor force onto the lowest partial waves. The changes fall to 20% only at $J = 4$. A comparison with the phase shift solutions reported by Stoks *et al.* [2] shows that these values are outside reasonable boundaries. Whereas results from single-energy analyses can oscillate rather widely and even reach values of ε_1 as high as 5°, such behavior is very different from the smooth one displayed by energy-dependent analyses. If only the shortest range Yukawa tensor term were to be adjusted, fitting the present data would require a value of ε_1 of 8.66°. To convey a more concrete idea of just how unacceptable this value is, we recall a phase shift analysis from the Basel group [52] which a number of years ago reported a value of nearly 3° for the $J = 1$ mixing parameter at 50 MeV. The question of whether this large value could be realistic was investigated [53] from various standpoints with the conclusion that the Basel result is most likely incorrect. In particular, it was argued that only a meson-exchange potential which includes no rho-meson contribution and uses an unrealistically small πNN cutoff mass (corresponding to a practically pointlike vertex), would be able to predict the Basel value. In conclusion, it is safe to say that the change in the tensor force apparently required by these measurements is inconsistent with NN data no matter how it is distributed among the NN partial waves. The small improvement obtained with the density-dependent case does not affect this conclusion.

TABLE I. Nucleon-nucleon mixing parameters.

J	Starting values	Fit to (n, p)	% increase
1	1.75°	5.02°	187
2	−2.22°	−2.81°	26
3	2.44°	3.01°	23
4	−0.34°	−0.41°	20

We have found that the energy-dependent renormalization of the tensor force that is needed to match the ^{10}B$(n, p)^{10}$Be(g.s.) cross sections at the lower energies is largely unaffected by changing to a finite-range DWIA calculation, applying the best modern interactions, or using the best available density-dependent DWIA model. On the other hand, if we assumed that the changes required could be accommodated by rescaling the NN tensor force, we would produce an interaction that would be inconsistent with the constraints from NN data.

Before we dismiss this as an isolated case found only in ^{10}B, it is important to consider whether there are other instances of such an anomalous energy dependence. We will restrict this search to only isovector, stretched transitions where the sensitivity to the effective NN interaction is essentially the same as it is in the ^{10}B$(n, p)^{10}$Be case that we have presented here. Figure 12 shows the cross section at the peak of the angular distribution for a number of isovector, stretched transitions. In the upper left panel, the ^{10}B$(n, p)^{10}$Be data as a function of energy from 70 to 200 MeV are shown with solid points connected by a dashed line to guide the eye. The highest energy point at 240 MeV was not included since the value at the peak was not measured and an estimate would have involved a long extrapolation using one of the DWIA calculations. The

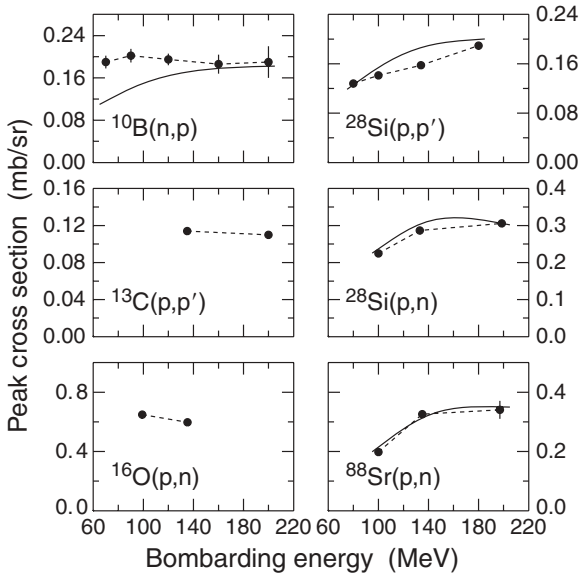

FIG. 12. Measurements of the peak cross section for a variety of nucleon-induced isovector, stretched transitions as a function of the nucleon bombarding energy. The left column shows data with a flat or falling energy dependence; the right column data with a rising energy dependence. The dotted lines are guides to the eye; the solid curves smoothly connect DWIA calculations for each set of data (if available). Further details about the data are given in the text.

solid line is the calculated energy dependence from DWIA using the modern free interaction. The failure of the upward trend in the calculation to match the almost energy independent ^{10}B$(n, p)^{10}$Be data was shown already by the ratios in Fig. 9.

To this comparison, we have added in the left-side column below the boron data two similarly energy-independent cases. In both cases, the cross section values are given at the peak of the angular distribution. There are two experiments that allow us to estimate what happens with the ^{13}C$(p, p')^{13}$C,$1/2^- \rightarrow 9/2^+$ transition [54–57]. These values, shown in the second panel, describe a flat or slightly declining cross section with increasing energy, the same as the trend for ^{10}B. A similar study of the ^{16}O$(p, n)^{16}$F, 4^- transition to the state at 6.37 MeV is shown in the third panel at 99 and 134 MeV [58]. (There are also measurements from Anderson [59] on the ^{48}Ca$(p, n)^{48}$Sc, 7^+ transition to the state at 1.10 MeV, but the values of the cross section at the peak for two energies are sufficiently close in value and beam energy that it is not possible to know whether the trend with energy it rising or falling.)

For nuclei heavier than these three cases, there are examples of an energy dependence in which the cross sections rise with increasing bombarding energy in accordance with the theoretical predictions. Among these are the studies of the 6^- isovector transition in ^{28}Si. Olmer reported ^{28}Si$(p, p')^{28}$Si cross section data at four energies between 80 and 180 MeV [60]. These are shown in the upper right panel along with the DWIA calculations (solid line). These data rise with rising energy, a trend that the DWIA predicts correctly. These DWIA calculations are very similar in energy dependence to those of the ^{10}B$(n, p)^{10}$Be reaction and reflect the energy dependence of this part of the effective NN interaction inside the DWIA mechanism. Pourang has reported ^{28}Si$(p, n)^{28}$P measurements that are shown in the second right-side panel along with DWIA calculations (solid line) [61]. Like the ^{28}Si$(p, p')^{28}$Si results, these cross sections also rise with energy. Pourang also reports similar results on the ^{88}Sr$(p, n)^{88}$Y, 9^+ transition to the state at 1.48 MeV (shown in the third right-side panel). Again, these cross sections rise with energy, as does the theory.

The phenomenon that we report for ^{10}B$(n, p)^{10}$Be appears to be a feature that is shared by other light mass nuclei. Thus there may be two kinds of isovector, tensor transitions. On medium mass nuclei, the cross section rises with increasing bombarding energy, but for nuclei with a mass less than about 20 the energy dependence is nearly flat. DWIA calculations predict a rising cross section in all cases, thus reproducing only the energy dependence of the medium mass cases.

There are a number of reaction mechanism issues that may become more important at lower mass and bombarding energy. The medium effects shown in Fig. 11 are large, and it may be the case that the nucleons involved as projectile and ejectile are more likely to penetrate deeply into the nucleus and still survive to contribute to this direct reaction when the target mass is light. This raises the possibility that relativistic effects, which were not explored here, might also be important. In this lighter mass region, the level density tends to be much smaller, and channel-coupling, which extends the impulse approximation beyond first order, may be more of a contributor at the lower energies. A study of the elastic scattering and natural parity excitations on ^{10}B$(p, p')^{10}$B found that coupling to the deformation of the target and the 4^+ state at 6.02 MeV was an important consideration [62]. (Unfortunately, we do not have computer programs that include both channel-coupling and full finite range capabilities within the same calculation.)

By using our energy dependent data, we now have a record of the onset of this failure of the DWIA as a function of the projectile energy. By looking to other similar cases, we also have defined the region in lighter target mass where this effect seems to appear consistently. This provides a boundary beyond which the standard DWIA calculation is no longer capable of producing an adequate description of the reaction (below 100 MeV and mass about 20). Additional theoretical investigations are needed to map out the extent of the problem more fully and to appreciate whether other effects not included in the present DWIA treatment are large enough and have the features needed to address this issue.

IV. CONCLUSIONS

We have presented the differential cross sections for the ^{10}B$(n, p)^{10}$Be(g.s.) reaction over the energy range from 70 to 240 MeV and at scattering angles from 20° to 44°. Initial zero-range calculations using the Franey-Love free interaction were not able to track the energy dependence of the measured cross sections. These cross sections were high relative to the calculations at 70 MeV and low at 240 MeV. Subsequent

calculations that addressed some questions about these initial results did not change this overall conclusion. Full finite range calculations reduced the discrepancy at the higher energies at the expense of making things worse at the lowest energy. The problem was reduced marginally with the incorporation of density dependence from Pauli blocking into the effective interaction. A separate inquiry into the consistency of such a large change to the tensor force led to the conclusion that the change was inconsistent with the constraints on the tensor force from NN scattering data. An examination of the energy dependence of other isovector stretched transitions in this mass and energy region has revealed that the flat energy dependence seen in this set of (n, p) cross section measurements is not unique to ^{10}B. Similar behavior is seen for the transitions in ^{13}C and ^{16}O. There are no other available cases until we reach the closed shell at ^{28}Si. But here the story changes: the measured cross sections rise with energy as does the theory. There is no problem with the DWIA here.

We conclude from these systematic comparisons with other experiments that there is no problem with the measurements reported here, rather the difficulty lies with theory. Since the limits of applicability for the DWIA seem to appear for lighter masses and lower energies, it is important to inquire what other physical processes might come into play. It is possible that a more complicated medium dependence is needed, but perhaps more likely that the reduced level density for the lighter mass targets leads to a greater role for channel-coupling effects in the cross section. Calculations with a theory that handles both coupling and finite range are needed to investigate this situation.

ACKNOWLEDGMENTS

We wish to thank J. A. Carr for his assistance with running ALLWRLD and a special thanks to F. Petrovich, who passed away on September 30, 2003, for his numerous contributions to nuclear theory and reactions. This work was supported in part by the U.S. Department of Energy under Contract Nos. W-7405-ENG-36, DE-AC05-76ER01067, DE-FG02-03ER41270 and the National Science Foundation Grant Nos. PHY-87-22008, PHY-88-102003, and PHY-01-00348.

[1] R. Satchler, *Direct Reactions* (Clarendon Press, Oxford, 1983), p. 642.
[2] V. G. J. Stoks, R. A. M. Klomp, M. C. M. Rentmeester, and J. J. de Swart, Phys. Rev. C **48**, 792 (1993).
[3] R. B. Wiringa, V. G. J. Stoks, and R. Schiavilla, Phys. Rev. C **51**, 38 (1995).
[4] R. Machleidt, Phys. Rev. C **63**, 024001 (2001).
[5] D. R. Entem and R. Machleidt, Phys. Rev. C **68**, 041001(R) (2003).
[6] S. W. Wissink *et al*., Phys. Rev. Lett. **83**, 4498 (1999).
[7] B. von Przewoski *et al*., Phys. Rev. C **58**, 1897 (1998).
[8] M. Sarsour *et al*., Phys. Rev. Lett. **94**, 082303 (2005).
[9] T. E. O. Ericson *et al*., Phys. Rev. Lett. **75**, 1046 (1995).
[10] K. Amos, P. J. Dortmans, H. V. von Geramb, S. Karataglidis, and J. Raynal, Adv. Nucl. Phys. **25**, 275 (2000).
[11] F. Sammarruca, E. J. Stephenson, and K. Jiang, Phys. Rev. C **60**, 064610 (1999).
[12] E. J. Stephenson, R. C. Johnson, and F. Sammarruca, Phys. Rev. C **71**, 014612 (2005).
[13] R. J. Furnstahl and S. J. Wallace, Phys. Rev. C **47**, 2812 (1993).
[14] F. Sammarruca, D. Alonso, and E. J. Stephenson, Phys. Rev. C **65**, 047601 (2002).
[15] R. Machleidt, Adv. Nucl. Phys. **19**, 189 (1989).
[16] W. G. Love, M. A. Franey, and F. Petrovich, in *Spin Excitations in Nuclei*, edited by F. Petrovich *et al*. (Plenum, New York, 1984), p.205.
[17] F. Sammarruca, E. J. Stephenson, K. Jiang, J. Liu, C. Olmer, A. K. Opper, and S. W. Wissink, Phys. Rev. C **61**, 014309 (2000).
[18] R. S. Hicks, J. Button-Shafer, B. Debebe, J. Dubach, A. Hotta, R. L. Huffman, R. A. Lindgren, G. A. Peterson, R. P. Singhal, and C. W. de Jager, Phys. Rev. Lett. **60**, 905 (1988).
[19] M. A. Franey and W. G. Love, Phys. Rev. C **31**, 488 (1985).
[20] R. A. Arndt, L. D. Roper, R. A. Bryan, R. B. Clark, B. J. VerWest, and P. Signell, Phys. Rev. D **28**, 97 (1983).
[21] P. W. Lisowski, C. D. Bowman, G. J. Russell, and S. A. Wender, Nucl. Sci. Eng. **106**, 208 (1990).
[22] D. S. Sorenson, Ph.D. thesis, University of California at Davis, CA 1990;J. Ullmann *et al*., LANL report LA-12061-T, May 1991.
[23] A. Ling *et al*., Phys. Rev. C **44**, 2794 (1991).
[24] R. A. Arndt and L. D. Roper, Scattering Analysis Interactive Dial-in (SAID) program (unpublished).
[25] J. F. Janni, Nucl. Data Tables **27**, 147 (1982).
[26] D. F. Measday and C. Richard-Serre, Nucl. Instrum. Methods **76**, 45 (1969).
[27] C. A. Goulding, Nucl. Instrum. Methods **153**, 511 (1978).
[28] J. A. Carr, F. Petrovich, D. Halderson, and J. Kelly, 1985 version of the computer program ALLWRLD (unpublished).
[29] J. A. Carr, F. Petrovich, D. Halderson, and J. Kelly, 1985 version of the computer program TAMURA (unpublished);and based on a version of the program VENUS from the ALLWRLD library.
[30] M. A. Schaeffer and J. Raynal, program DWBA81, as modified by S. M. Austin, W. B. Love, J. R. Comfort, and C. Olmer (private communication).
[31] H. Baghaei *et al*., Phys. Rev. Lett. **69**, 2054 (1985).
[32] A. W. Carpenter, F. Petrovich, R. J. Philpott, and J. A. Carr (to be published).
[33] A. W. Carpenter, Ph.D. thesis, Florida State University, 1988.
[34] C. W. Glover *et al*., Phys. Rev. C **41**, 2487 (1990).
[35] C. W. Glover *et al*., Phys. Rev. C **43**, 1664 (1991).
[36] H. V. von Geramb, in *The Interaction between Medium Energy Nucleons in Nuclei*, AIP Conf. Proc. 97, edited by H. O. Meyer (AIP, New York, 1983), p. 44.
[37] L. Rikus, K. Nakano, and H. V. von Geramb, Nucl. Phys. **A414**, 413 (1984).
[38] S. Cohen and D. Kurath, Nucl. Phys. **73**, 1 (1965).
[39] M. A. Franey and W. G. Love, Phys. Rev. C **31**, 488 (1985).
[40] P. R. Lewis *et al*., Nucl. Phys. **A532**, 583 (1991).
[41] P. R. Lewis, Ph.D. thesis, University of Melbourne, 1990.
[42] R. A. Lindgren, W. J. Gerace, A. D. Bacher, W. G. Love, and F. Petrovich, Phys. Rev. Lett. **42**, 1524 (1979).

[43] F. Petrovich *et al*., Phys. Lett. **B95**, 166 (1980).
[44] T. de Forest, Jr. and J. D. Walecka, Adv. Phys. **15**, 1 (1966).
[45] F. Petrovich and W. G. Love, addendum to the LAMPF Workshop on Pion Single Charge Exchange, LASL Report LA-7892-C (1979).
[46] F. Petrovich, in *The (p,n) Reaction and the Nucleon-Nucleon Force*, edited by C. D. Goodman *et al*. (Plenum, New York, 1980), p. 115.
[47] V. G. J. Stoks, R. A. M. Klomp, C. P. F. Terheggen, and J. J. de Swart, Phys. Rev. C **49**, 2950 (1994).
[48] J. J. Kelly, program manual for LEA, 1995.
[49] H. de Vries, C. W. de Jager, and C. de Vries, At. Data Nucl. Data Tables **36**, 495 (1987).
[50] M. I. Haftel and F. Tabakin, Nucl. Phys. **A158**, 1 (1970).
[51] W. G. Love and M. A. Franey, Phys. Rev. C **24**, 1073 (1981).
[52] M. Hammans *et al*., Phys. Rev. Lett. **66**, 2293 (1991).
[53] R. Machleidt and I. Slaus, Phys. Rev. Lett. **72**, 2664 (1994).
[54] S. F. Collins, G. G. Shute, B. M. Spicer, V. C. Officer, I. Morrison, K. A. Amos, D. W. Devins, D. L. Friesel, and W. P. Jones, Nucl. Phys. **A380**, 445 (1982).
[55] S. F. Collins, G. G. Shute, B. M. Spicer, V. C. Officer, K. A. Amos, D. W. Devins, D. L. Friesel, and W. P. Jones, Nucl. Phys. **A481**, 494 (1988).
[56] L. Rikus *et al*., Aust. J. Phys. **35**, 9 (1982).
[57] W. M. Schmitt *et al*., IUCF Sci. and Tech. Report, May 1993–April 1994, p. 23.
[58] A. Fazely *et al*., Phys. Rev. C **25**, 1760 (1982).
[59] B. D. Anderson, T. Chittrakarn, A. R. Baldwin, C. Lebo, R. Madey, R. J. McCarthy, J. W. Watson, B. A. Brown, and C. C. Foster, Phys. Rev. C **31**, 1147 (1985).
[60] C. Olmer, A. D. Bacher, G. T. Emery, W. P. Jones, D. W. Miller, H. Nann, P. Schwandt, S. Yen, T. E. Drake, and R. J. Sobie, Phys. Rev. C **29**, 361 (1984).
[61] R. Pourang *et al*., Phys. Rev. C **44**, 689 (1991).
[62] A. C. Betker *et al*., Phys. Rev. C **71**, 064607 (2005).